JOURNAL OF SOLID STATE CHEMISTRY 137, 283–288 (1998)
ARTICLE NO. SC977735

Structure of $Pb^{II}Sn^{IV}(PO_4)_2$: Stereochemical Activity of the Lead II Lone Pair

E. Morin[1], G. Wallez, S. Jaulmes, J. C. Couturier, and M. Quarton

Laboratoire de Cristallochimie du Solide, CNRS URA 1388, Université Pierre et Marie Curie, 4, place Jussieu, 75252 Paris Cedex 05, France

Received July 29, 1997; in revised form December 8, 1997; accepted December 15, 1997

Flux-grown single crystals of the new compound $PbSn(PO_4)_2$ have been studied by X-ray diffraction. It crystallizes in monoclinic space group $P2_1/n$ (No. 14), with cell parameters $a = 4.861(6)$ Å, $b = 14.75(2)$ Å, $c = 8.80(2)$ Å, $\beta = 93.0(1)^\circ$, $Z = 4$. Its structure is related to the yavapaiite type with a skeleton made up of corner-linked SnO_6 octahedra and PO_4 tetrahedra, but the lead atoms are located in double tunnels instead of sheets. An active Pb^{II} lone pair has been localized from electrostatic interactions in order to explain this original structure.

INTRODUCTION

The monophosphates are a promising field of investigations as hosting materials for lithium intercalation because of the numerous open structures discovered among them which allow high ionic mobility. We have studied compounds in the Pb^{II}–Sn^{IV}–P–O system and their tin mixed-valence derivatives, expecting that the Pb^{II} lone pair would create original open structures. Among the various possible formulae, we attempted to characterize the $Pb^{II}Sn^{IV}(PO_4)_2$ compound, assumed to crystallize under the noncompact yavapaiite form $KFe(SO_4)_2$ (1) as all other known $A^{II}B^{IV}(PO_4)_2$ derivates (A = Ca, Sr, Ba; B = Ge, Sn, Ti, Zr, Hf, Mo) (2–4). This paper reports the original structure of this new monophosphate and the stereochemical activity of the Pb^{II} lone pair.

PREPARATION OF CRYSTALS

Single crystals of the compound were flux-grown in a platinum crucible from a melt of $PbSn(PO_4)_2$ (12.5% molar) in SnP_2O_7. Both flux and compound are obtained *in situ* from SnO_2, $PbCO_3$, and $NH_4H_2PO_4$. The charge was slowly cooled (5°C/h) from 1100 to 800°C, then faster (20°C/h) to room temperature. Obtained crystals are transparent and colorless with an hexagonal prismatic shape. Chemical composition is confirmed by X-ray fluorescence analysis which shows a Pb:Sn:P ratio close to 1:1:2.

STRUCTURE DETERMINATION

Weissenberg and precession photographs, obtained from a $PbSn(PO_4)_2$ single crystal, made it possible to identify the space group as $P2_1/n$. Collection of diffracted intensities was performed at 20°C on a Syntex-Nicolet P3F four-circle diffractometer. Main data collection parameters are summarized in Table 1.

Collected intensities were first corrected of Lorentz and polarization factors. Crystal morphology and dimensions have been verified from ψ-scan measurements on five planes, then used for absorption corrections with N. W. Alcock's analytical method (5, 6).

Lead atom was first located from the three-dimensional Patterson maps and its position was refined with an isotropic temperature factor. Electronic density maps obtained from Fourier series gave approximate coordinates of tin, phosphorus, and oxygen. Then, refinements of atomic coordinates (Table 2) and anisotropic displacement parameters (Table 3) were performed by means of a modified ORXFLS program (7) using atomic scattering factors (8). Secondary extinction corrections show spherical domains with gaussian distribution in size and a medium radius of 0.6×10^{-3} mm (type II according to P. Becker and P. Coppens (9)). The final anisotropic refinement yielded the reliability factors $R = 0.054$ and $R_w = 0.058$. These values are somewhat high, but satisfactory considering the presence of heavy atoms in the formula.

STRUCTURE DESCRIPTION

The three-dimensional structure is based upon an alternate succession of SnO_6 octahedra and PO_4 tetrahedra. The SnO_6 unit is vertex-connected to six PO_4; one oxygen atom of each tetrahedron has one unshared vertex. Pb^{II} cations take place in the so-formed cavities (Fig. 1). The framework appears fairly related to the yavapaiite type (1).

[1] To whom correspondence should be addressed.

0022-4596/98 $25.00

TABLE 1
Crystallographic and Experimental Data

Crystal data	
Formula	$PbSn(PO_4)_2$
Formula weight (g mol^{-1})	515.82
Crystal dimensions (mm)	$0.58 \times 0.11 \times 0.07$
a (Å)	4.861(6)
b (Å)	14.75(2)
c (Å)	8.80(2)
β (deg)	93.0(1)
V (Å^3)	630.1(1)
Space group	$P2_1/n$ (No. 14)
Z	4
D calc. (g cm^{-3})	5.44
$F(000)$	904
μ (Mo$K\alpha$) (mm^{-1})	44.8
Data collection	
Scan mode	θ–2θ
Scan angle	2θ ranges: $2\theta_1 - 1.0^\circ$ to $2\theta_2 + 1.0^\circ$, θ_1 and θ_2 being the diffraction angles for Mo$K\alpha_1$ and $K\alpha_2$ radiations
Recording angular range θ (°)	2.6–30
hkl range	$-6 \le h \le 6$; $0 \le k \le 20$; $0 \le l \le 12$
Number of independent data	1848 measured
Reflections with $I > \sigma(I)$	1420 used in refinements
Structure solution and refinement	
Extreme values of transmission factor	0.031–0.160
Number of variables	110 (including anisotropic temperature factors for all atoms)
$R = \sum \lvert\lvert F_o\rvert - \lvert F_c\rvert\rvert / \sum F_o$	0.054
Weighting scheme	$w = 1/\sigma(F)$
$R_w = [\sum w \cdot (F_o - \lvert F_c\rvert)^2 / \sum w . F_o^2]^{1/2}$	0.058
Extinction parameter refined	$g = 0.85(9) \times 10^{-6}$
Extreme residual electronic density	$\Delta\rho_{min} = -1.4$; $\Delta\rho_{max} = 3.6$ e Å^{-3}

PO_4 tetrahedra are fairly regular, with average P–O bond lengths equal to 1.55 Å for P(1) and 1.53 Å for P(2) (Table 4). The sum of bond strengths around phosphorus atoms, calculated by applying the empirical model of Brown and Wu (10) based on the oxygen–cation distance, is close to 5 valence units as expected: 4.92 for P(1) and 5.08 for P(2). The short P(1)–O(1) and P(2)–O(5) distances correspond to bonds with oxygen atoms which are not linked to tin

TABLE 2
Fractional Atomic Coordinates and Thermal Parameters
$U_{eq} = 1/3 \sum_i \sum_j U_{ij} a_i^* a_j^* a_i \cdot a_j$

Atom	x	y	z	U_{eq} (10^{-3} Å^2)
Pb	0.2195(2)	0.09920(5)	0.09245(8)	17.4(3)
Sn	0.2366(3)	0.35844(7)	0.0485(1)	11.3(5)
P(1)	0.285(1)	0.7635(3)	0.1100(5)	13(2)
P(2)	0.758(1)	0.4760(3)	0.2045(5)	12(2)
O(1)	0.157(3)	0.8499(9)	0.048(2)	24(7)
O(2)	0.566(3)	0.7503(8)	0.037(1)	17(6)
O(3)	0.100(3)	0.6781(8)	0.083(1)	18(6)
O(4)	0.150(3)	0.2682(8)	0.214(1)	17(6)
O(5)	0.754(3)	0.9937(8)	0.126(1)	21(6)
O(6)	0.642(3)	0.5615(8)	0.125(1)	16(6)
O(7)	0.062(3)	0.4627(7)	0.162(2)	19(6)
O(8)	0.595(3)	0.3905(8)	0.162(1)	17(6)

TABLE 3
Anisotropic Displacement Parameters (10^{-3} Å^2)

	U_{11}	U_{22}	U_{33}	U_{12}	U_{13}	U_{23}
Pb	23.2(4)	15.1(3)	13.5(3)	4.1(3)	−3.0(2)	−1.0(3)
Sn	13.2(6)	10.1(5)	10.6(5)	−0.3(4)	−0.1(4)	0.0(4)
P(1)	16(3)	12(2)	12(2)	0(2)	−1(2)	−0(2)
P(2)	16(3)	10(2)	12(2)	0(2)	1(2)	−0(2)
O(1)	21(8)	21(7)	28(8)	5(6)	−5(6)	2(6)
O(2)	21(7)	10(5)	18(6)	−0(5)	−1(6)	−0(5)
O(3)	23(7)	18(6)	13(6)	0(5)	−4(6)	−0(5)
O(4)	24(7)	17(6)	8(6)	−8(5)	−3(5)	0(5)
O(5)	43(9)	6(5)	14(6)	1(6)	−8(6)	4(5)
O(6)	20(7)	16(6)	15(6)	2(5)	9(5)	3(5)
O(7)	25(8)	8(5)	22(7)	−3(5)	−2(6)	3(5)
O(8)	17(7)	12(6)	20(6)	−5(5)	1(5)	−1(5)

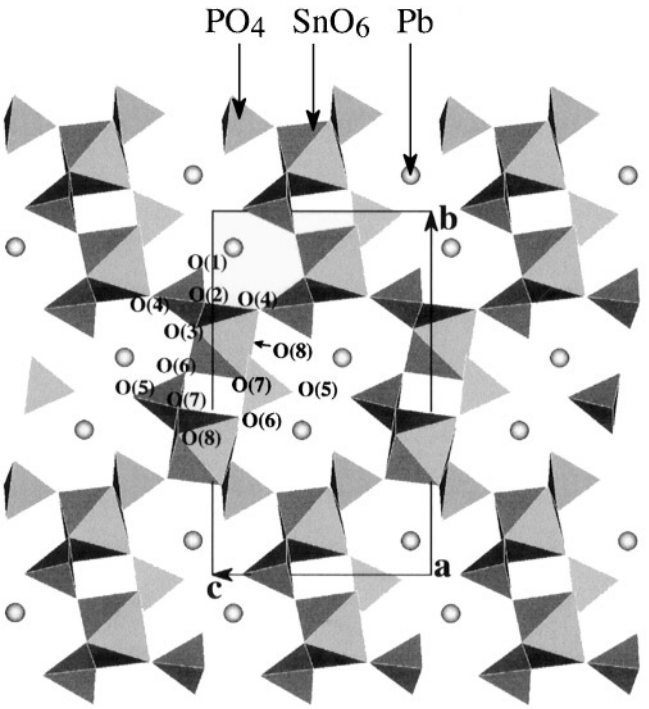

FIG. 1. Cell projection of $PbSn(PO_4)_2$.

(Table 4) and which present the largest thermal parameters (Table 2).

The SnO_6 octahedron is very regular too. Sn–O distances are a little bit short with an average of 2.03 Å (Table 4).

TABLE 4
Distances (Å) and Angles (°) in $P(1)O_4$, $P(2)O_4$ and SnO_6 Polyhedra

P(1)	O(1)	O(2)	O(3)	O(4)		
O(1)	1.51(1)	108.2(7)	113.9(7)	112.3(7)		
O(2)	2.48(2)	1.55(1)	110.5(7)	106.0(7)		
O(3)	2.57(2)	2.56(2)	1.56(1)	105.7(7)		
O(4)	2.55(2)	2.49(2)	2.49(2)	1.57(1)		
P(2)	O(5)	O(6)	O(7)	O(8)		
O(5)	1.52(1)	105.8(7)	110.3(7)	109.8(7)		
O(6)	2.44(2)	1.53(1)	109.1(7)	113.1(7)		
O(7)	2.52(2)	2.52(2)	1.56(1)	108.8(7)		
O(8)	2.49(2)	2.55(2)	2.51(2)	1.53(1)		
Sn	O(2)	O(3)	O(4)	O(6)	O(7)	O(8)
O(2)	2.03(1)	87.7(5)	82.4(5)	91.0(5)	172.4(5)	87.4(5)
O(3)	2.81(2)	2.03(1)	92.5(5)	89.0(5)	97.8(5)	174.0(5)
O(4)	2.68(2)	2.93(2)	2.03(1)	173.2(5)	92.1(5)	90.4(5)
O(6)	2.91(2)	2.85(2)	4.07(2)	2.04(1)	94.2(5)	87.5(5)
O(7)	4.07(2)	3.07(2)	2.93(2)	2.99(2)	2.04(1)	87.3(5)
O(8)	2.80(2)	4.04(2)	2.88(2)	2.81(2)	2.80(2)	2.02(1)

TABLE 5
Distances Around Pb Atom and Lone Pair *E*, *E*–Pb–O Angles

	Pb core–O (Å)	*E*–O (Å)	*E*–Pb–O (°)
O(1)	2.28(1)	2.75	131
O(5)	2.37(1)	2.92	146
O(2)	2.72(1)	2.93	102
O(4)	2.74(1)	2.51	63
O(5)	2.77(1)	2.95	99
O(5)	3.03(1)	2.95	77
O(7)	3.10(1)	2.72	49
O(3)	3.16(1)	2.55	14
O(6)	3.16(1)	2.83	54
	$\langle Pb–O \rangle = 2.81$ sd = 0.33	$\langle E–O \rangle = 2.79$ sd = 0.17	

Indeed, the cumulated bond strengths for tin cations gives 4.37 v.u. with a contribution of the furthest oxygen anion of 0.71 v.u.

The larger lead atom occupies sites in the ***a***-oriented double tunnels of the oxygen framework. The coordination polyhedron is irregular and the number of nine neighbors was determined by computation of bond strengths, showing that lead is surrounded by a tricapped trigonal prism (Table 5, left-hand column). The bond strength sum (1.98 v.u.) is in good agreement with the theorical valence of the cation (2.04 with 10 neighbors). So the 10th neighbor, which is more than 3.41 Å away, may be dismissed.

LONE PAIR LOCALIZATION

Anisotropy of bond lengths in the environment of heavy p-block cations M^{m+} with electronic external configuration $ns^2\ np^0$ is known as "lone pair effect." It is generally admitted that some hybridization occurs between ns and np orbitals if the M^{m+} concentration is high enough, forming an off-centered space-filling entity able to play the role of an additional anion. Compound $PbSn(PO_4)_2$ appears as an interesting case because the length difference between extreme PbO bonds indicates a far greater lone pair stereochemical activity than expected on the basis of the rather high volume per lead atom (157.5 $Å^3$).

The general problem that makes difficult the localization of lone pairs by diffraction methods is their low electronic density and their closeness to the core of the heavy M^{m+} cation. Therefore, Verbaere *et al.* (11) have proposed a calculation process based upon electrostatic interactions in which the high polarizability of the "$ns^2\ np^0$" cation is supposed to be mainly due to the presence of a lone electron pair. So the lone pair-core dipolar momentum is roughly equal to the induced polarization **P**,

$$\mathbf{P} = -2 \cdot \mathbf{d} = \boldsymbol{\alpha} \cdot \mathbf{E},$$

TABLE 6
Lone Pair (*E*) Position

E fractional coordinates		$x = 0.257$	$y = 0.105$	$z = 0.163$
Core–*E* distance (Å)	$d = 0.64$	$d_x = 0.18$	$d_y = 0.09$	$d_z = 0.62$
Shortest *E*–*E* distances (Å)	4.83 ($\times 1$)	4.86 ($\times 2$)	4.91 ($\times 1$)	

where -2 is the charge of the lone pair, **d** the core–lone pair distance, $\alpha = 6.58$ Å^3 the polarizability of lead II (12), and **E** the local electrostatic field calculated by Ewald's method (13). This formula is used by the laboratory-made program HYBRIDE to compute the electrostatic field on the lead atoms, giving the approximate coordinates of the lone pairs which are taken into account in the field calculatation of the next loop until self-consistent positions are reached.

Because $PbSn(PO_4)_2$ could not be considered as ionic, it was more realistic to consider atom partial charges instead of oxidation states. Mean ionicity of each kind of cation–oxygen bond (14) was calculated from the electronegativity difference of the terminal atoms (15) and applied to the oxidation states of the cations, giving charges $+2.19$ for tin and $+2.01$ for phosphorus. Lead cation, with a global $+1.23$ charge was introduced as a mobile -2 for the lone pair and a fixed $+3.23$ representing the nucleus and core orbitals. Although occupying slightly different sites, oxygen anions were given identical balancing charges of -0.93. Calculation reached a self-consistent position (Table 6) for the barycenter of the lone pair about 0.64 Å apart from the core center, nearly at the same *y* coordinate.

STEREOCHEMICAL ACTIVITY OF THE LONE PAIR

Figure 2, along with lead–oxygen and lone pair–oxygen distances and lone pair-lead-oxygen angles listed in Table 5, shows the typical features of a stereochemically active lone pair: Pb atom is strongly off-centered in its coordination polyhedron (0.55 Å apart from the oxygen barycenter) while the lone pair lies near the center (0.28 Å), with more regular distances to the neighbor oxygen atoms (2.51 to 2.95 Å). Considering the lone pair as a nearly spherical entity and its distances to atoms O(3), O(6), and O(7) located "in front" of it, we can estimate its radius as about 1.34 Å, nearly the same as for an oxygen anion. In the opposite direction, the metal–oxygen distances are very short (2.28 and 2.37 Å) and nearly equal to normal lead IV–oxygen distances (2.30 Å for an eightfold coordination) (16).

Describing the structure of yellow PbO, Galy *et al.* (17) suggested that the Pb^{II} lone pairs and the oxygen atoms build up together some kind of hexagonal compact anionic packing in which the remaining Pb^{IV} entities adopt a low coordination. The same remark applies to red PbO, but in this case, lone pairs and oxygen atoms form a tetragonal

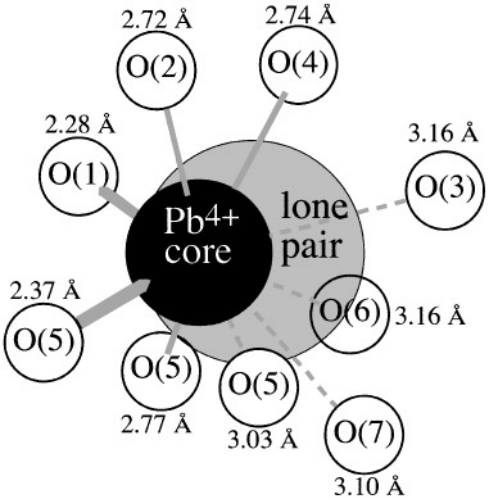

FIG. 2. View of the tricapped PbO_9 prism. Lead core orbitals have been given the size of a Pb^{4+} cation. Lone pair volume and shape are those of an oxygen anion.

body-centered sublattice. In both cases, lone pair positions calculated with HYBRIDE confirmed this model. The behavior of the lone pair in $PbSn(PO_4)_2$ is similar, even if the shape of the coordination polyhedron is less regular than in the two forms of PbO: with its central position, the hybridized $6s^2$ orbital takes a full part in the anionic packing.

One can wonder why $PbSn(PO_4)_2$ does not crystallize under the yavapaiite $KFe(SO_4)_2$ type (1) adopted by all known $A^{II}B^{IV}(PO_4)_2$ compounds (2–4) (Fig. 3). As the ionic radius of Pb^{II} (1.29 Å) is close enough to those of Ca^{II} (1.12 Å), Sr^{II} (1.26 Å), and Ba^{II} (1.42 Å) (16), any size effect can be dismissed and only the stereochemical properties induced by the lone pair have to be considered. Indeed, the main difference comes from the environment of the big cations:

— in the yavapaiite type, slabs of corner-linked tetrahedra and octahedra alternate with layers of large nearly-spherical alkali or alkali-earth cations showing a roughly hexagonal disposition (4×4.82 Å and 2×5.15 Å);

— this disposition is not favorable to lead II atoms because dense electronic clouds would repel each other. In $PbSn(PO_4)_2$, similar polyhedra build zigzag tunnels in which each lead atom only has four lead neighbors: one very close (3.92 Å) and three further ones (1×4.37 Å and 2×4.86 Å) (Fig. 4). In this way, they form a nearly hexagonal packing of lone pairs (1×4.83 Å, 2×4.86 Å, and 1×4.91 Å) enabled by the tunnel shape which allows them to occupy side positions (Fig. 1 and 3b).

Galy *et al.* (17) pointed out that s^2 pairs are stereochemically active only when the stoïchiometric M^*/M ratio is high (M^* is the lone pair bearer, M represents the other cations); that is, if the environment of M^* is not imposed by

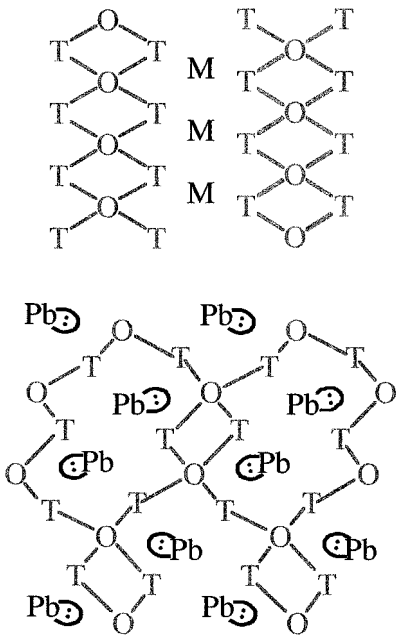

FIG. 3. Idealized structural patterns of Yavapaiite (a) and $PbSn(PO_4)_2$ (b). *T* and O represent the oxygen tetrahedra and octahedra respectively; M and Pb the interstitial cations. Note that M are disposed in layers, Pb in double tunnels.

framework-forming MX_n polyhedra. In $PbSn(PO_4)_2$, the lead atoms in the double tunnels are locally predominant, resulting in lone pairs nearly as active as in red PbO but with a four times higher cell volume per lead atom.

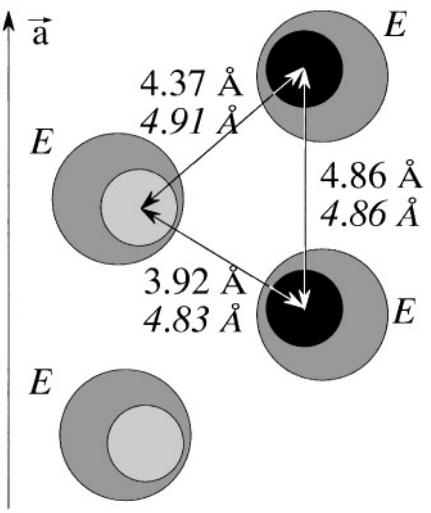

FIG. 4. (011) projection of lead cores and lone pairs in the *a*-oriented tunnels. Lone pairs are shown as light grey spheres with distances values in italics; lead cores are black (in front of the lone pairs) or light grey spheres (behind) with distances values in right types.

DISCUSSION

Although the hybridization of the $6s^2$ orbital and the irregularity of the lead–oxygen distances are definitely correlated, their relationship could appear as a chicken-and-egg problem: is the anisotropic environment the consequence of the polarization of the lead electron cloud or does the latter result from the former? Computing the lone pair position from classical structural data (coordinates of the core of the bearer and of the other atoms) may wrongly suggest that the lone pair is just a floating space-filling entity along the direction of the electrostatic field. Actually, the repulsions between the electronic clouds of the Pb^{II} cation and its neighbors are lowered by decomposition in a bulky negatively charged lone pair and a small and strongly positive Pb^{IV} fictive cation. The lone pair is slightly shifted away from the center of the oxygen polyhedron by the core which inserts into the so-formed cavities and only plays a minor steric role.

Thus, the self-consistent field method must be seen as a way to define the equilibrium position of an electric dipole of which the only previously known extremity (the core) is the biggest in term of electronic density but not the most prominent in term of steric role. Core–oxygen, lone pair–oxygen, and lone pair–lone pair distances fully agree with the simple steric model based upon a virtual splitting of cation Pb^{II} into Pb^{IV} and an oxygen-like lone pair. This model also applies to other heavy ns^2np^0 cations as thallium I, tin II, antimony III, bismuth III, and tellurium IV.

CONCLUSION

The structure of $PbSn(PO_4)_2$, solved from single-crystal diffraction data appears as an original alteration of the common yavapaiite structure: lead atoms are hosted in zigzag tunnels instead of layers as a result of the stereochemical activity of the lone pair. This compound also highlights the possibility of a lone pair activity even with a high volume per lead atom, provided that the layout of the bearers is inhomogeneous enough to build up chains or clusters.

ACKNOWLEDGMENTS

The authors thank Mr. A. Mazurier (Laboratoire de Physique, Faculté de Pharmacie, Université Paris V) for performing the diffracted intensities collection.

REFERENCES

1. E. J. Graeber and A. Rosenzweig, *Am. Mineral.* **56,** 1917 (1972).
2. R. Masse and A. Durif, *C. R. Acad. Sci. Paris Sér. C* **274,** 1692 (1972).
3. M. Th. Paques-Ledent, *J. Inorg. Nucl. Chem.* **39,** 11 (1977).
4. A. Leclaire, M. M. Borel, J. Chardon, and B. Raveau, *J. Solid State Chem.* **116,** 364 (1995).

5. N. W. Alcock, *in* "Crystallographic Computing," p. 271, Munksgaard, Copenhagen, 1970.
6. J. De Meulenaer and H. Tompa, *Acta Crystallogr. Sect. A* **19**, 1014 (1965).
7. W. R. Busing, *Acta Crystallogr. Sect. A* **27,** 683 (1971).
8. "International Tables for X-Ray Crystallography," Vol. IV. Kynoch Press, Birmingham, 1974.
9. P. Becker and P. Coppens, *Acta Crystallogr. Sect. A* **30,** 129 (1974).
10. I. D. Brown and K. K. Wu, *Acta Crystallogr. Sect. B* **32,** 1957 (1976).
11. A. Verbaere, R. Marchand, and M. Tournoux, *J. Solid State Chem.* **23,** 383 (1978).
12. R. D. Shannon, *J. Appl. Phys.* **73**, 348 (1993).
13. P. P. Ewald, *Ann. Phys.* **64,** 253 (1921).
14. L. Pauling, "The Nature of the Chemical Bond." Cornell Univ. Press, New York, 1939.
15. A. L. Allred and E. G. Rochow, *J. Inorg. Nucl. Chem.* **5,** 264 (1958).
16. R. D. Shannon, *Acta Crystallogr. Sect. A* **32,** 751 (1976).
17. J. Galy, G. Meunier, S. Anderson, and A. Åström, *J. Solid State Chem.* **13,** 142 (1975).